Check for updates

# Doppler-free spectroscopy with a terahertz quantum-cascade laser

## M. WIENOLD,[1,2,*] T. ALAM,[1] L. SCHROTTKE,[3] H. T. GRAHN,[3] AND H.-W. HÜBERS[1,2]

[1]*German Aerospace Center (DLR), Institute of Optical Sensor Systems, Rutherfordstr. 2, 12489 Berlin, Germany*
[2]*Humboldt-Universität zu Berlin, Department of Physics, Newtonstr. 15, 12489 Berlin, Germany*
[3]*Paul-Drude-Institut für Festkörperelektronik, Leibniz-Institut im Forschungsverbund Berlin e. V., Hausvogteiplatz 5–7, 10117 Berlin, Germany*
[*]*martin.wienold@dlr.de*

**Abstract:** We report on the Doppler-free saturation spectroscopy of a molecular transition at 3.3 THz based on a quantum-cascade laser and an absorption cell in a collinear pump-probe configuration. A Lamb dip with a sub-Doppler linewidth of 170 kHz is observed for a rotational transition of HDO. We found that a certain level of external optical feedback is tolerable as long as the free spectral range of the external cavity is large compared to the width of the absorption line.

## References and links

1. M. S. Vitiello, L. Consolino, S. Bartalini, A. Taschin, A. Tredicucci, M. Inguscio, and P. De Natale, "Quantum-limited frequency fluctuations in a terahertz laser," Nat. Photonics **6**, 525–528 (2012).
2. J. L. Kloosterman, D. J. Hayton, Y. Ren, T. Y. Kao, J. N. Hovenier, J. R. Gao, T. M. Klapwijk, Q. Hu, C. K. Walker, and J. L. Reno, "Hot electron bolometer heterodyne receiver with a 4.7-THz quantum cascade laser as a local oscillator," Appl. Phys. Lett. **102**, 011123 (2013).
3. H. Richter, M. Wienold, L. Schrottke, K. Biermann, H. T. Grahn, and H.-W. Hübers, "4.7-THz local oscillator for the GREAT heterodyne spectrometer on SOFIA," IEEE Trans. Terahertz Sci. Technol. **5**, 539–545 (2015).
4. D. Büchel, P. Pütz, K. Jacobs, M. Schultz, U. U. Graf, C. Risacher, H. Richter, O. Ricken, H.-W. Hübers, R. Güsten, C. E. Honingh, and J. Stutzki, "4.7-THz superconducting hot electron bolometer waveguide mixer," IEEE Trans. Terahertz Sci. Technol. **5**, 207–214 (2015).
5. C. Risacher, R. Güsten, J. Stutzki, H. W. Hübers, D. Büchel, U. U. Graf, S. Heyminck, C. E. Honingh, K. Jacobs, B. Klein, T. Klein, C. Leinz, P. Pütz, N. Reyes, O. Ricken, H. J. Wunsch, P. Fusco, and S. Rosner, "First supra-THz heterodyne array receivers for astronomy with the SOFIA observatory," IEEE Trans. Terahertz Sci. Technol. **6**, 199–211 (2016).
6. L. Rezac, P. Hartogh, R. Güsten, H. Wiesemeyer, H.-W. Hübers, C. Jarchow, H. Richter, B. Klein, and N. Honingh, "First detection of the 63 $\mu$m atomic oxygen line in the thermosphere of Mars with GREAT/SOFIA," Astron. Astrophys. **580**, L10 (2015).
7. J. Remillard, D. Uy, W. Weber, F. Capasso, C. Gmachl, A. Hutchinson, D. Sivco, J. Baillargeon, and A. Cho, "Sub-Doppler resolution limited Lamb-dip spectroscopy of NO with a quantum cascade distributed feedback laser," Opt. Express **7**, 243–248 (2000).
8. N. Mukherjee, R. Go, and C. K. N. Patel, "Linewidth measurement of external grating cavity quantum cascade laser using saturation spectroscopy," Appl. Phys. Lett. **92**, 111116 (2008).
9. S. Bartalini, S. Borri, and P. De Natale, "Doppler-free polarization spectroscopy with a quantum cascade laser at 4.3 $\mu$m," Opt. Express **17**, 7440–7449 (2009).
10. R. J. Walker, J. Kirkbride, J. H. van Helden, D. Weidmann, and G. A. D. Ritchie, "Sub-Doppler spectroscopy with an external cavity quantum cascade laser," Appl. Phys. B **112**, 159–167 (2013).
11. J. C. Pearson, B. J. Drouin, A. Maestrini, I. Mehdi, J. Ward, R. H. Lin, S. Yu, J. J. Gill, B. Thomas, C. Lee, G. Chattopadhyay, E. Schlecht, F. W. Maiwald, P. F. Goldsmith, and P. Siegel, "Demonstration of a room temperature 2.48–2.75 THz coherent spectroscopy source," Rev. Sci. Instrum. **82**, 093105 (2011).
12. G. Cazzoli and C. Puzzarini, "Sub-Doppler resolution in the THz frequency domain: 1 kHz accuracy at 1 THz by exploiting the Lamb-dip technique," J. Phys. Chem. A **117**, 13759–13766 (2013).

13. L. Consolino, A. Campa, M. Ravaro, D. Mazzotti, M. S. Vitiello, S. Bartalini, and P. De Natale, "Saturated absorption in a rotational molecular transition at 2.5 THz using a quantum cascade laser," Appl. Phys. Lett. **106**, 021108 (2015).

14. M. Wienold, L. Schrottke, M. Giehler, R. Hey, W. Anders, and H. T. Grahn, "Low-voltage terahertz quantum-cascade lasers based on LO-phonon-assisted interminiband transitions," Electron. Lett. **45**, 1030–1031 (2009).

15. H. M. Pickett, R. L. Poynter, E. A. Cohen, M. L. Delitsky, J. C. Pearson, and H. S. P. Müller, "Submillimeter, millimeter, and microwave spectral line catalog," J. Quant. Spectrosc. Radiat. Transfer **60**, 883–890 (1998).

16. W. Demtröder, *Laser spectroscopy*, vol. 2 (Springer, 2008).

17. V. S. Letokhov and V. P. Chebotayev, *Nonlinear laser spectroscopy* (Springer, 1977).

18. H. Richter, S. G. Pavlov, A. D. Semenov, L. Mahler, A. Tredicucci, H. E. Beere, D. A. Ritchie, and H.-W. Hübers, "Submegahertz frequency stabilization of a terahertz quantum cascade laser to a molecular absorption line," Appl. Phys. Lett. **96**, 071112 (2010).

19. N. van Marrewijk, B. Mirzaei, D. Hayton, J. R. Gao, T. Y. Kao, Q. Hu, and J. L. Reno, "Frequency locking and monitoring based on bi-directional terahertz radiation of a 3rd-order distributed feedback quantum cascade laser," J. Infrared Millim. Terahertz Waves **36**, 1210–1220 (2015).

20. H.-W. Hübers, H. Richter, R. Eichholz, M. Wienold, K. Biermann, L. Schrottke, and H. T. Grahn, "Heterodyne spectroscopy of frequency instabilities in terahertz quantum-cascade lasers induced by optical feedback," IEEE J. Sel. Top. Quantum Electron. **23**, 1800306 (2017).

21. R. Lang and K. Kobayashi, "External optical feedback effects on semiconductor injection laser properties," IEEE J. Quantum Electron. **QE-16**, 347–355 (1980).

22. A. D. Rakić, T. Taimre, K. Bertling, Y. L. Lim, P. Dean, D. Indjin, Z. Ikonić, P. Harrison, A. Valavanis, S. P. Khanna, M. Lachab, S. J. Wilson, E. H. Linfield, and A. G. Davies, "Swept-frequency feedback interferometry using terahertz frequency QCLs: a method for imaging and materials analysis," Opt. Express **21**, 22194–22205 (2013).

23. M. Wienold, T. Hagelschuer, N. Rothbart, L. Schrottke, K. Biermann, H. T. Grahn, and H.-W. Hübers, "Real-time terahertz imaging through self-mixing in a quantum-cascade laser," Appl. Phys. Lett. **109**, 011102 (2016).

## 1. Introduction

Nonlinear laser spectroscopy enables to overcome limitations in molecular spectroscopy regarding spectral resolution. The absorption of laser radiation by molecules changes the population density of the involved states. At larger intensities, this leads in turn to saturation and nonlinear absorption features. A prominent example is the observation of a Lamb dip in the center of an inhomogeneously broadened absorption line, which can be exploited for high-resolution spectroscopy and frequency stabilization. In order to perform nonlinear saturation spectroscopy, lasers with narrow-band emission are required. At terahertz (THz) frequencies, quantum-cascade lasers (QCLs) are suitable because they are powerful continuous-wave sources with a quantum-limited intrinsic linewidth of the order of 100 Hz [1]. This makes them ideal sources for spectroscopic applications requiring ultimate frequency resolution as in the fields of THz metrology and THz remote sensing of gaseous species. Employed as local oscillators, QCLs have enabled a new class of heterodyne spectrometers for frequencies up to 4.7 THz [2–5]. The spectral resolution of such an instrument becomes limited by the frequency stability of the laser system. For the present 4.7-THz heterodyne receiver of the *Stratospheric Observatory For Infrared Astronomy* (SOFIA), the achievable resolution is currently on the order of a few MHz [6], which approaches already the molecular Doppler broadening under typical laboratory conditions. In order to circumvent the Doppler limit, precision spectroscopy on a sub-MHz frequency scale requires a nonlinear spectroscopic technique in addition to a stable laser source.

While in recent years Doppler-free saturation spectroscopy based on QCLs has been successfully established in the mid-infrared spectral region [7–10], previous results in the THz range are solely based on upconversion of microwave sources [11, 12]. While optical saturation with a QCL was already reported in an earlier study for a transition of methanol at 2.5 THz, no Doppler-free spectra were obtained [13]. Due to the much narrower absorption lines as compared to the mid-infrared range, challenges for Doppler-free spectroscopy are the required pump power in combination with a sufficiently small linewidth of the laser source and a sensitive detection method. Here, we report on true Lamb dip spectroscopy in a collinear pump-probe configuration based on a free-running QCL at 3.3 THz, a free-space absorption cell, and a Ge:Ga photo-conductive detector. This approach may also be suitable for Lamb dip frequency stabilization of QCLs.
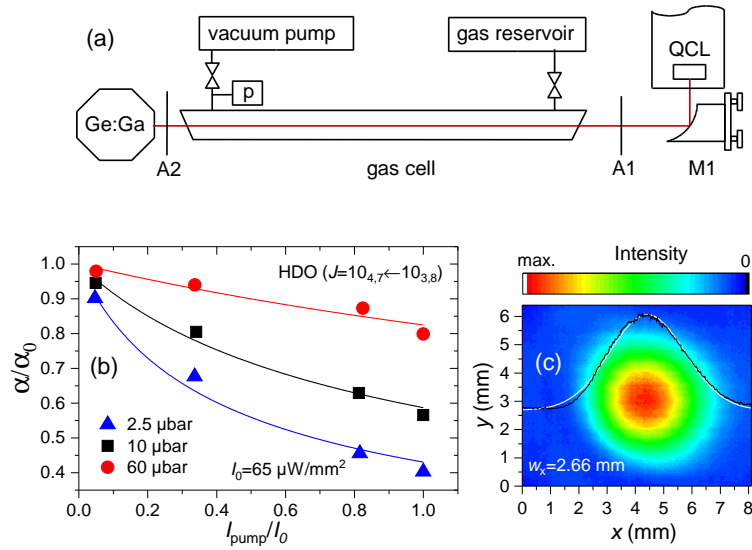
Fig. 1. (a) Schematics of the setup for linear absorption spectroscopy and saturation measurements. M1: off-axis parabolic mirror; p: pressure gauge; A1, A2: attenuators. (b) Normalized absorption coefficient $\alpha/\alpha_0$ as a function of the normalized pump intensity $I_{\text{pump}}/I_0$ for different values of the total pressure. The solid lines refer to a fit to Eq. (1) with the following parameters: $\alpha_0 = 7.4\times10^{-4}$ cm$^{-1}$ and $I_s/I_0 = 0.23$ for 2.5 $\mu$bar; $\alpha_0 = 3.9\times10^{-3}$ cm$^{-1}$ and $I_s/I_0 = 0.53$ for 10 $\mu$bar; $\alpha_0 = 2.2\times10^{-2}$ cm$^{-1}$ and $I_s/I_0 = 2.1$ for 60 $\mu$bar. (c) Intensity profile of the QCL at the beam waist position. The solid lines refer to a central cut in the horizontal direction (black) and the corresponding fit to a Gaussian distribution (white).

## 2. Experimental configuration for saturation spectroscopy

The employed QCL is based on a *bound-to-continuum* active region with phonon-assisted electron injection [14], which emits a single mode at 3.3 THz with up to 1 mW of continuous-wave output power. In a first step, the QCL emission was characterized by Fourier-transform spectroscopy in order to verify single-mode operation and to determine the emission frequency with a precision of about 5 GHz. In a second step, laser absorption spectroscopy was performed for a more precise frequency calibration based on methanol (CH$_3$OH) with its well-documented fingerprint spectrum as a reference [3]. The corresponding setup is illustrated in Fig. 1(a). The QCL is either operated in a liquid-He flow cryostat or in a mechanical cryocooler. The beam is collected with an off-axis parabolic mirror, and the transmitted radiation is measured with a Ge:Ga photo-conductive detector after passing through a 60-cm-long gas cell. The absorption spectra are obtained by sweeping the driving current of the QCL for different settings of the heat sink temperature. For the present laser, we identified a suitable single-mode frequency range of 3.309–3.312 THz with tuning parameters of −170 MHz/K and +8 MHz/mA at a current scan rate of 2 A/s. In the our case, scan rates between 1–2 A/s represented a good compromise for minimizing low-frequency flicker noise and maintaining a sufficient frequency resolution for Doppler-free measurements. In a typical configuration, the current is scanned from below threshold over the entire dynamic range of single-mode operation, resulting in acquisition times of 100–200 ms/scan.

For saturation spectroscopy, the molecular species was changed to deuterated water (in an isotopic ratio of H:D:$^{16}$O=1:1:1), which exhibits fewer but stronger absorption lines than methanol

within the available frequency range. A particularly strong rotational transition in the vicinity of the laser power maximum was identified as the $J = 10_{4,7} \leftarrow 10_{3,8}$ transition of single-deuterated water (HDO) at 3.311835 THz [15]. For this transition, we determined the saturation intensity and the unsaturated absorption coefficient from power-dependent measurements by attenuating the pump power in front of the gas cell with a rotating wire grid. Figure 1(b) displays the normalized absorption coefficient as a function of the normalized pump intensity for different values of the total pressure. The solid lines refer to respective parameter fits according to the equation for an inhomogeneously broadened transition given by

$$\alpha = \frac{\alpha_0}{\sqrt{(1 + I_{pump}/I_s)}} \, , \tag{1}$$

where $\alpha$ denotes the absorption coefficient, $\alpha_0$ the unsaturated absorption coefficient, $I_{pump}$ the pump intensity, and $I_s$ the saturation intensity [16]. As expected, the absorption becomes less saturated toward higher pressures. For the lowest pressure of 2.5 $\mu$bar, which was also used for Doppler-free experiments, we determined values of $\alpha_0 = (7.4 \pm 0.4) \times 10^{-4}$ cm$^{-1}$ and $I_s = (0.23 \pm 0.05)I_0$, where $I_0$ denotes the unattenuated pump intensity. By comparing the unsaturated absorption coefficient to a molecular data base, [15] we infer a partial pressure of $(0.58 \pm 0.03)$ $\mu$bar for HDO. This value differs from the total pressure due to the coexistence of non- and double-deuterated water molecules. In order to determine the power density $I_0$, we measured the beam profile as well as the total power. The beam profile in the focal plane, as acquired with a microbolometer camera, is depicted in Fig. 1(c). The intensity distribution is well described by a Gaussian profile with beam waist parameters of $w_x = 2.66$ mm and $w_y = 2.80$ mm, where $w_x$ and $w_y$ denote the standard deviation in the horizontal and vertical direction, respectively. From total power measurements with a THz power meter (Thomas Keating), we infer a maximum pump power of 0.76 mW in the gas cell, corresponding to a peak pump power density of $I_0 = 65$ $\mu$W/mm$^2$.

## 3. Lamb dip spectroscopy

For Doppler-free spectroscopy, the optical setup was modified according to Fig. 2(a). A collinear probe beam is generated by a plane mirror after the gas cell. A wire grid polarizer (WGP) is used in combination with a quarter-wave ($\lambda/4$) plate made from $x$-cut quartz to deflect the probe beam to the detector and to reduce the impact of external optical feedback to a tolerable amount. In order to avoid detector saturation, the beam is further attenuated after the gas cell. In such a configuration with counter-propagating waves, the observable Lamb dip is well described by the rate equation approach described in [17], Letokhov and Chebotayev. In the limit of $I_{probe} \ll I_{pump} \ll I_s$, where $I_{probe}$ denotes the probe intensity, the absorption coefficient of the probe is given by

$$\alpha = \alpha_0 \left( 1 - \frac{S}{2} \frac{(\Gamma/2)^2}{(\nu - \nu_0)^2 + (\Gamma/2)^2} \right) \, . \tag{2}$$

Here, $S$ denotes the saturation parameter, $\nu$ the laser frequency, $\nu_0$ the central frequency, and $\Gamma$ the full width at half maximum (FWHM) of the transition in the absence of Doppler broadening, i.e. the sub-Doppler linewidth. The saturation parameter is given by $S = I_{pump}/I_s$. At larger saturation levels for which $I_{pump}$ is no longer small compared to $I_s$, the parameters $S$ and $\Gamma$ in Eq. (2) have to be replaced by

$$S \rightarrow \tilde{S} = \frac{2S}{1 + S + \sqrt{1 + S}} \, , \tag{3}$$

$$\Gamma \rightarrow \tilde{\Gamma} = \frac{\Gamma}{2} \left( 1 + \sqrt{1 + S} \right) \, . \tag{4}$$
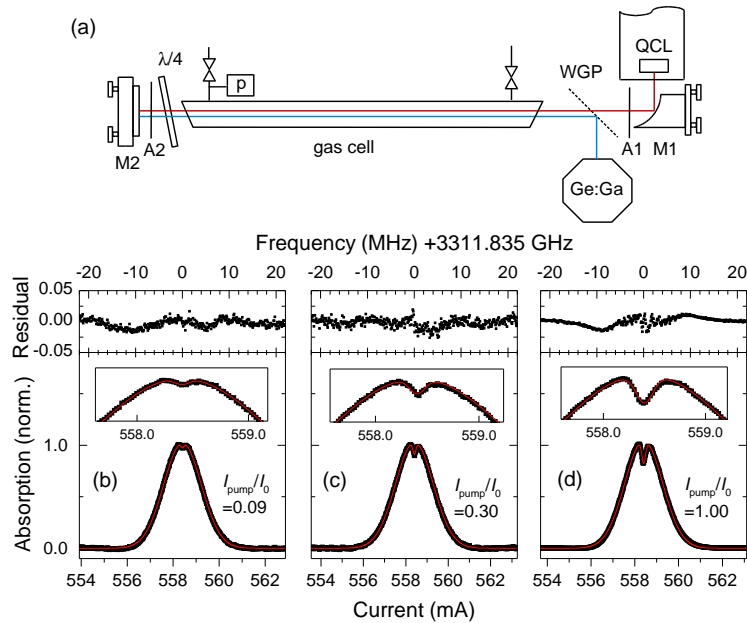
Fig. 2. (a) Setup for Doppler-free spectroscopy. WGP: wire grid polarizer, $\lambda/4$: quarter-wave plate. (b)–(d) Lower panels: normalized absorption signal for different intensities of the pump beam as a function of the driving current for a total pressure of 2.5 $\mu$bar. Dots refer to the experimental data (averaged over 19 scans with a current scan rate of 1 A/s at 30 K), while the solid lines show results of simulations according to Eqs. (2)–(5). The simulation parameters are: $S = 4.3$, $\Gamma = 170$ kHz, $\gamma_{\text{QCL}} = 700$ kHz [$\gamma_{\text{QCL}} = 800$ kHz in (d)]. Upper panels: residuals, i.e. differences between measured and simulated spectra. The relative frequency scale has been assigned according to the Doppler width (FWHM of 9.42 MHz) of the unsaturated transition.

Hence, the spectral width of the Lamb dip depends on the saturation parameter, which is known as power broadening. If the linewidth of the laser is not negligible with respect to the Lamb dip, the absorption has to be convoluted with the normalized line profile $I(\nu)$ of the laser ($\int_0^\infty I(\nu)d\nu = 1$):

$$\alpha_{\text{eff}}(\nu) = (\alpha * I)(\nu) . \tag{5}$$

A Lamb dip will be observed if its spectral width is comparable or larger than the linewidth of the laser, whereby its amplitude and shape depend on the parameters $S$, $\Gamma$, and the QCL linewidth. Note that both, the width and the depth of the Lamb dip, are affected by $\Gamma$ through the convolution according to Eq. (5), since the spectral area of the Lamb dip, which is proportional to $\tilde{S}\,\tilde{\Gamma}$, is conserved.

Experimental results for the $J = 10_{4,7} \leftarrow 10_{3,8}$ transition of HDO are shown in Figs. 2(b)–2(d) for different pump intensities. For these measurements, the QCL was operated in the flow cryostat. Due to detection noise, an averaging over 19 sweeps was performed for a reliable quantitative analysis of the data. This corresponds to an averaging time of 2.3 s. As expected, the observed Lamb dip becomes deeper with increasing pump power. From the analysis of the data, we can estimate $\Gamma$ as well as the width of the laser line, since both affect the shape of the Lamb dip in different ways. While the dots in Figs. 2(b)–2(d) refer to the experimental data, the solid lines display results of the simulations according to Eqs. (2)–(5) assuming a Gaussian lineshape for the QCL. For a saturation parameter of $S = 4.3$ as obtained from Fig. 1(b), we determined a

sub-Doppler linewidth of $\Gamma = (170 \pm 30)$ kHz and a FWHM of $\gamma_{QCL} = (750 \pm 150)$ kHz for the QCL line taking into account the uncertainty of the method. The effective linewidth of the QCL is hence much larger than the intrinsic Shawlow-Townes limit, which can be below 100 Hz for THz QCLs [1].

By operating the QCL in a flow cryostat, the experimental configuration is free from mechanical vibrations. The QCL linewidth, which enters Eq. (5), becomes then determined by the temperature fluctuations over the averaging time of 2.3 s. According to the temperature tuning coefficient of $-170$ kHz/mK, a linewidth of 750 kHz corresponds to a temperature stability of $\pm 2.2$ mK, which is in agreement with the stability level of our temperature control loop. A minor contribution might also result from the accuracy of the current ramp; the actual step size of 22 $\mu$A in Figs. 2(b)–2(d) corresponds to about 100 kHz in frequency. Fluctuations due to the intrinsic noise of the employed current source (Wavelength Electronics, QCL1000) are expected to be negligible for the present configuration.

The determined sub-Doppler linewidth $\Gamma$ is slightly larger than expected for transit time and collisional broadening. For a transit time broadening due to the finite beam size, we would expect a FWHM of $\Delta \nu_{transit} = 0.4 \, v \, w \approx 50$ kHz for a beam waist of $w = 2.8$ mm and a mean molecule velocity of $v = 360$ m/s at 300 K [16]. In case of collisional broadening, we would expect a sub-Doppler linewidth of 40 kHz according to the self-broadening coefficient of 16 MHz/mbar. The discrepancy between this value and the experimentally determined value of $\Gamma$ may be explained by the spatially inhomogeneous pump power density and an only partial overlap between the pump and the probe beam, which is not taken into account in the analysis. Hence, the values for the sub-Doppler and the QCL linewidth should be considered as upper limits. From the first derivative of the absorption signal shown in Fig. 2(d), we identified a suitable frequency range of $\pm 350$ kHz for a Lamb dip stabilization loop. Compared with the frequency locking to an unsaturated absorption peak [18, 19], we expect an improvement of the frequency stability from a few hundred kHz to a few tens of kHz.

## 4. Doppler-free spectroscopy in the presence of cooler vibrations and optical feedback

Finally, we briefly elucidate the impact of cooler vibrations and external optical feedback for Doppler-free measurements. Most application scenarios rely on mechanical cryocoolers instead of flow cryostats [3]. This typically implies a significant level of cooler vibrations, which were identified as a source of frequency fluctuations [18, 20]. We found that a Lamb dip signal is still observable under such conditions, if the measurement is synchronized to the fundamental frequency of the cooler vibration. In our case, vibrations are dominated by the 45-Hz piston cycle of the employed Stirling cooler (Ricor, model K535). By synchronizing the measurement to the piston cycle, fluctuations at the fundamental vibration frequency are suppressed to a large extent. The remaining fluctuations at higher-order vibration frequencies can be tolerated, if the acquisition time for the spectral range of interest is made sufficiently short ($\leq 10$ ms). Vibration-induced flicker noise does then mainly appear as a scan-to-scan lateral offset in the spectra, which can be compensated by a post-acquisition jitter correction routine. In our case, the limiting factor is the sampling rate of the acquisition and control hardware (50 kHz), which restricts the maximum current scan rate to about 2 A/s in order to maintain a sufficiently small frequency step for Lamb dip spectroscopy.

The optical setup as shown in Fig. 2(a) suppresses optical feedback already to a large extent. However, residual feedback might be caused by unintended spurious reflections as well as by the limited efficiency of the quarter-wave plate and the wire grid polarizer. Actually, we found that even a rather strong optical feedback can be tolerated in our setup. This is due to a peculiarity of the THz range, where the free spectral range of the external cavity can be large compared to the Doppler width of a molecular absorption line. The level of optical feedback can be adjusted by
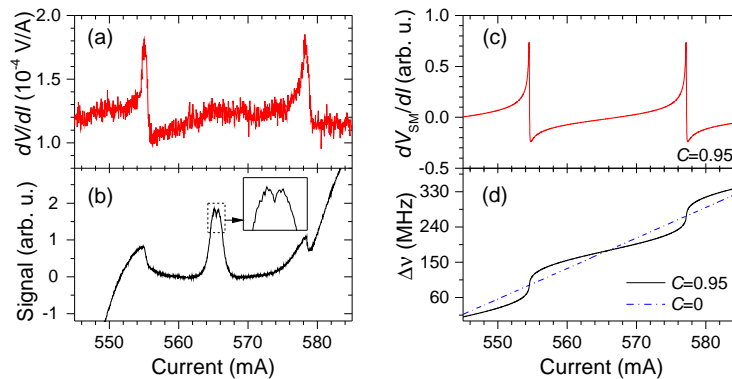
Fig. 3. Lamb dip spectroscopy in the presence of optical feedback. The QCL was operated in a Stirling cooler at 35 K. (a) First derivative of the measured QCL voltage (single scan, 2A/s) and (b) measured detector signal after baseline subtraction as a function of the driving current. (c) Simulated derivative of the self-mixing voltage component and (d) simulated frequency shift in the presence of optical feedback as a function of the driving current. The simulation parameters are $C = 0.95$ for the feedback parameter and $\alpha_{\mathrm{LEF}} = -0.2$ for the linewidth enhancement factor.

rotating the quarter-wave plate. One indication of optical feedback is then found in the operating voltage of the QCL, which contains a feedback-related self-mixing component. Figure 3(a) depicts the first derivative of the QCL voltage in the presence of optical feedback. A periodic self-mixing component is found, where the periodicity reflects the 175-MHz free spectral range of the optical cavity formed by the QCL and the mirror after the gas cell. The corresponding absorption signal after third-order polynomial baseline subtraction is depicted in Fig. 3(b). The Lamb dip is clearly observed within the absorption peak. Two additional features (at 555 and 578 mA) are observed in the absorption signal, which are correlated to the self-mixing voltage spikes in Fig. 3(a) and caused by the external-cavity resonances. In order to better understand this result and to estimate the level of optical feedback, we performed simulations based on the Lang-Kobayashi model for external optical feedback [21–23]. The results of such a simulation are depicted in Figs. 3(c) and 3(d). A good agreement with the observed self-mixing voltage signature is found for a feedback parameter of $C = 0.95$. This value is already close to the intermediate feedback regime ($C > 1$), for which the system becomes bistable. As depicted in Fig. 3(d), optical feedback causes a modulation of the undisturbed frequency-current dependence with a linear range in the center of each modulation period. For Lamb dip spectroscopy, the molecular absorption line should ideally appear at the center of this linear range. Experimentally, this can be achieved by adjusting the external cavity length, where in our case a mirror displacement of 22 $\mu$m shifts the modulation by one half of the period. Note that optical feedback effects have not been observed for the measurements shown in Fig. 2.

## 5. Summary and conclusion

In summary, we demonstrated Doppler-free spectroscopy based on a THz QCL and a free-space gas cell in a collinear pump-probe configuration. The results clearly show that a sub-MHz laser linewidth is achievable for measurements with a free-running QCL even for integration times of several seconds. In case of operation in a vibration-free flow cryostat, the QCL linewidth becomes limited by the achievable temperature and current stability. We further found that a certain level of stationary optical feedback is tolerable for Doppler-free measurements as long

as the free spectral range for the optical cavity is large compared to the width of the molecular absorption line. The presented results may be useful for future Lamb dip stabilization of QCLs and Doppler-free precision spectroscopy based on devices which are phase locked to an electronic or optical frequency reference.